JOURNAL OF GEOPHYSICAL RESEARCH, VOL. 108, NO. E4, 8034, doi:10.1029/2002JE001876, 2003

Correction published 3 July 2003

Design and field experiments of a ground-penetrating radar for Mars exploration

Carl Leuschen,[1] Pannir Kanagaratnam,[2] Kenji Yoshikawa,[3] Steve Arcone,[4] and Prasad Gogineni[2]

Received 15 February 2002; revised 24 April 2002; accepted 31 July 2002; published 20 March 2003.

[1] We developed a wideband, low-power, lightweight, prototype ground-penetrating radar (GPR) for subsurface exploration for Mars. The transmitter and receiver subsystems were constructed using a commercially available radio frequency (RF) and digital integrated circuits, connectorized components, and evaluation boards. The transmit/receive system, antennas, laptop controller, and batteries are all accommodated on a 2.5-m sled. Field experiments were conducted in Kansas and Alaska. The experiments in Kansas tested the operation of the system. The primary objective of the Alaska experiments was to investigate the ability of a GPR to detect and distinguish between subsurface deposits of ice and ice-cemented soils. The investigation depths of these experiments ranged from 1 m to 30 m, and the subsurface geology included near-surface thaw, discontinuous permafrost, water-saturated soils, and lenses of pure ice. Dielectric contrasts within the ground were detected with near-meter resolution; however, identifying the geologic context of an interface was difficult due to ambiguities associated with reflection data. These investigations demonstrate some of the difficulties associated with inverting reflection data to obtain dielectric properties of the subsurface. Fortunately, previous geophysical investigations such as drilled cores and seismic surveys helped to constrain the geology, and numerical simulations provided an additional resource for the interpretations. On Mars, additional geological context will be limited and numerical simulations will become extremely important for data interpretation. Due to these difficulties, we demonstrate in one experiment how dielectric information can be obtained directly from bistatic measurements with a fixed transmitter and mobile receiver. Finally, a comparison with a commercially available Geophysical Survey Systems, Inc. (GSSI) radar system is presented, and we discuss how the system can be modified and improved for future exploration on Mars. *INDEX TERMS:* 0910 Exploration Geophysics: Data processing; 0925 Exploration Geophysics: Magnetic and electrical methods; 0994 Exploration Geophysics: Instruments and techniques; 1823 Hydrology: Frozen ground; *KEYWORDS:* Ground-penetrating radar (GPR), Mars, analog, measurements, permafrost

Citation: Leuschen, C., P. Kanagaratnam, K. Yoshikawa, S. Arcone, and P. Gogineni, Design and field experiments of a ground-penetrating radar for Mars exploration, *J. Geophys. Res.*, *108*(E4), 8034, doi:10.1029/2002JE001876, 2003.

1. Introduction

[2] Using ground-penetrating radars to investigate the subsurface of Mars will be a key scientific objective over the next several years, especially in light of the large possibility that water could exist within the planet. Radars operating from a few megahertz up to a gigahertz will be able to provide valuable information concerning the subsurface structure at resolutions ranging from a few centimeters near the surface to a few tens of meters at greater depths. The specific design and acquirable information of a system will depend on many factors, such as the desired geographic coverage, host spacecraft specifications, mission objectives, and depth of investigation. One important consideration that should not be overlooked is that the electrical properties of the subsurface of Mars are, for the most part, unknown. In order to ensure the successful operation of a ground-penetrating radar in these unknown conditions on Mars, the system specifications, most importantly the operating frequency and bandwidth, must be designed to cover a broad range.

[3] Currently, the state of the art for ground-penetrating radars consists of impulsive systems that require high-power pulses and small duty cycles. One of the major technical goals of the presented work was to develop a lightweight, low-power, frequency-modulated radar system that could be

[1]Applied Physics Laboratory, Johns Hopkins University, Laurel, Maryland, USA.
[2]Radar Systems and Remote Sensing Laboratory, University of Kansas, Lawrence, Kansas, USA.
[3]Water and Environmental Research Center, Institute of Northern Engineering, University of Alaska, Fairbanks, Fairbanks, Alaska, USA.
[4]USACE Engineer Research and Development Center, Cold Regions Research and Engineering Laboratory, Hanover, NH, USA.

0148-0227/03/2002JE001876$09.00

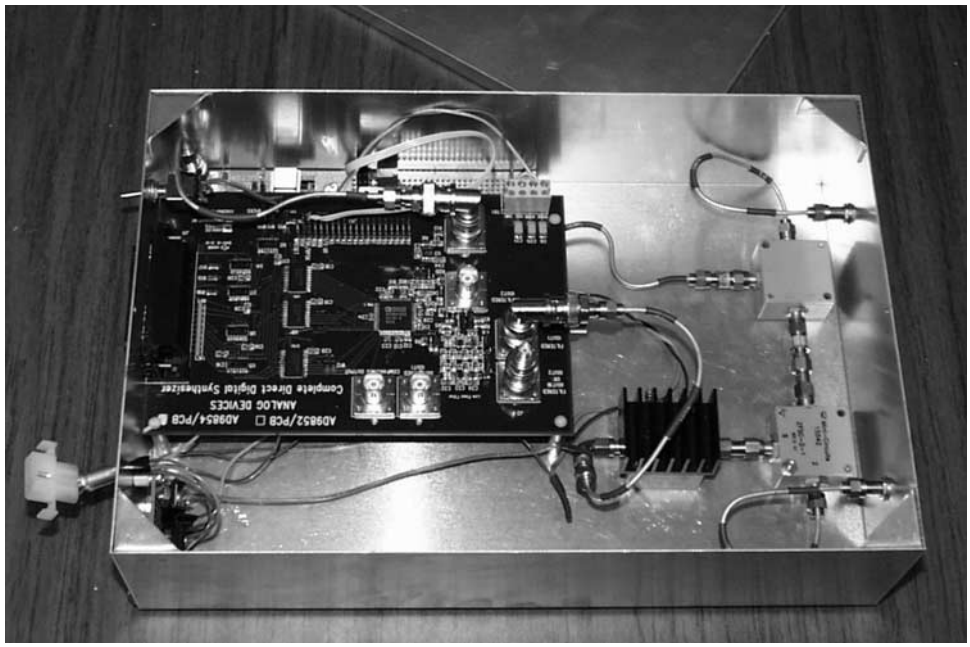

Figure 1. Prototype transmitter/receiver subsystem.

used to detect subsurface deposits of ice and water. The radar was designed to operate from 5 MHz to 120 MHz to achieve adequate depth penetration while retaining near-surface resolution. Our objective was to design a simple system that could acquire information in a variety of environments and still be miniaturized to meet spacecraft requirements. This paper begins by outlining the complete design and construction of the system, including the transmitter/receiver and antenna subsystems. A preliminary field experiment was conducted in Kansas to verify the operation of the prototype system. Next, field experiments conducted over permafrost and ice in Alaska are presented.

2. Radar System

[4] We constructed a simple ground-penetrating radar system to serve as a test bed to investigate radar performance, system trade-offs, signal processing, data interpretation, and antenna subsystems. The prototype was built with off-the-shelf evaluation boards and connectorized components. It uses a direct digital synthesizer and can generate a variety of waveforms, including a simple pulse, chirped pulse, FMCW or other modulated signals. A chirped pulse waveform was used to achieve low peak power, high average power, and fine resolution. This section describes the basic construction and operation of the transmitter and receiver, and a few possible configurations for the antenna subsystems.

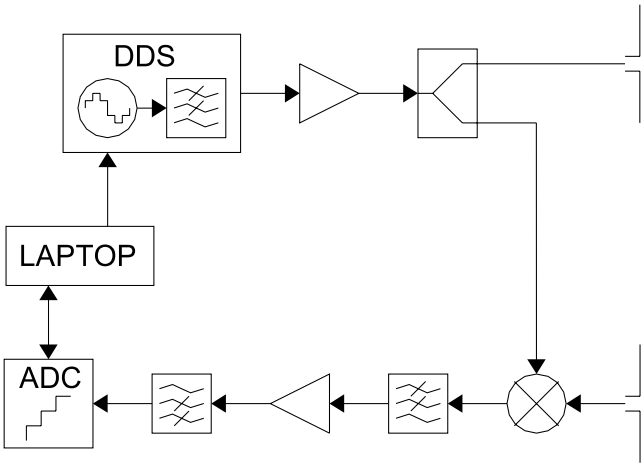

Figure 2. Prototype system block diagram.

2.1. Transmitter/Receiver

[5] The prototype transmitter and receiver subsystem is shown in Figure 1, the block diagram of the system is shown in Figure 2, and the specifications are listed in Table 1. The basic operation of the system is summarized as follows. The transmitter generates a 5-MHz to 120-MHz chirp signal after receiving a trigger from the system controller. The transmitter is capable of generating frequencies down to D.C., but 5 MHz is the lower bound of the transmit antenna. This chirp signal is generated using a 300-MHz direct digital synthesizer (DDS). Higher-order harmonics generated by the DDS digital-to-analog con-

Table 1. System Specifications[a]

Parameter	Description
Modulation	Swept-FM, Stepped-FM, Pulsed
Frequency	Programmable up to 120 MHz
Sweep Time (Pulse Width)	Programmable
Power Output	10 dBm
Total Power Consumption	<3 Watts
ADC Resolution	16 bits
ADC Dynamic Range	96 dB
ADC Sampling Rate	2.5 MSPS
Size	7 cm × 20 cm × 30 cm
Weight	1.5 kg

[a]Excluding antennas, batteries, and laptop.

verter are reduced using an elliptical low-pass filter with a cut-off frequency of 120 MHz that corresponds to 40% of the 300-MHz clock. The signal is amplified with a high-power amplifier, and the amplified signal is split into two parts, one for the transmit antenna and the other to serve as the local oscillator for a mixer that is used to de-chirp the received signal. Due to the digital-to-analog conversion, the transmit signal exhibits a $\sin(t)/t$ roll-off as the signal is swept from 5 MHz to 120 MHz.

[6] The receiver demodulates the input radio-frequency (RF) response into an intermediate-frequency (IF) signal and digitizes the resulting waveform. The IF signal is obtained by mixing a replica of the transmit signal with the receive signal, producing a collection of beat frequency signals, each proportional to the product of the sweep rate and corresponding time delay of the reflector. These signals are low-pass filtered to remove the higher frequency components generated by the mixer. After low-pass filtering, a single-pole high-pass filter provides attenuation of the direct antenna coupling and an increased gain for the weak subsurface returns. This high-pass filter is analogous to range gating or time controlled gain in an impulsive radar system. The high-pass output is amplified and then digitized by a 2.5-MSPS 16-bit analog-to-digital converter.

[7] All timing and control of the system are accomplished through the parallel port of a laptop computer and with a few low-speed digital integrated circuits. Evaluation software was used to trigger the system and store the data to memory. Unfortunately, the evaluation software did not include software drivers to automate this process, and data collection was relatively slow. Excluding batteries and the antenna subsystems, the system weighs about 1.5 kg with dimensions of 7 cm by 20 cm by 30 cm, as shown in Figure 1. The complete system could be easily miniaturized using a printed circuit board and surface mount components to satisfy weight and volume constraints of a rover.

[8] To aid in data collection, a second transmitter/receiver system was constructed using a 16-bit 50-kSPS PCMCIA data-acquisition card. The card came with software drivers to develop automated control interface using National Instruments LabVIEW graphical programming development software. The timing and data acquisition were accomplished through one of the PCMCIA ports of a laptop computer, and the DDS was programmed through the parallel port of the computer. The relatively low speed of the data acquisition card significantly reduced the maximum sweep rate of the system. Also, since the analog-to-digital converter was inside the computer (rather than inside the shielded aluminum case for the original system), the analog IF signal was sent over a ribbon cable from the receiver to the laptop. This non-shielded PCMCIA cable also carried the timing signals for the digital part of the system and picked up interference from the digital components and power supplies. The new system offered an improvement in the rate of data collection at the cost of higher noise interference.

2.2. Antenna Subsystems

[9] With ground-penetrating radar, there is a trade-off between range resolution and penetration depth [*Davis and Annan*, 1989]. This trade-off is largely due to the antenna subsystems and their limited bandwidths. High-frequency antennas are often needed to achieve the large bandwidths and fine resolution. Higher frequencies suffer from increased attenuation and result in poor penetration depth. Alternatively, lower frequencies must be used to get the desired depth penetration resulting in smaller bandwidths, and therefore, the resolution of the system is sacrificed.

[10] Another problem is the size of the antenna, especially for a rover on Mars. Even if resolution is not a necessity, there is still a limitation on the size of an antenna that can be accommodated on a rover. Electrically small antennas can be used, but they commonly exhibit a very large reactance (either capacitive or inductive depending on the type of antenna), a low radiation resistance, and a high quality-factor (Q-factor) resulting in a narrow bandwidth. Due to these characteristics, matching a small antenna over a broad frequency range is extremely difficult and resistive components are often used.

[11] For example, a ground-penetrating radar using resistively loaded dipole antennas typically has a relative bandwidth of 40%. A 10-MHz center-frequency system may be needed to achieve reasonable penetration to detect ice on Mars. This results in a 15-m antenna with a 4-MHz bandwidth and a resolution on the order of 40 m. In contrast, a 190-MHz system would be needed to achieve a resolution of 2 m. Looking at these numbers and the tradeoffs discussed in the previous two paragraphs, antenna design will likely be the most important aspect of the radar system development. In the next few sections, the antennas for both the transmitter and receiver of the radar system will be analyzed, starting with the effects of placing an antenna on a lossy ground.

2.2.1. Antenna on a Lossy Ground

[12] A number of loading effects are noticed when an antenna is placed directly on the ground. First, due to the dielectric loading of the ground, the frequency response of the antenna will be shifted down and the radiation resistance will decrease. This decrease of the resonant frequency will allow proportionally smaller antennas to be used for the same frequency range. Second, the Q-factor of the system will be lowered and there will be an increase in bandwidth if the ground exhibits electrical loss [*Fujimoto et al.*, 1987]. This is similar to resistively loading an antenna. Finally, the dielectric half-space will alter the far-field radiation characteristics of the antenna by focusing most of the energy into the ground and producing nulls along the air-ground interface and peaks at the critical angles [*Annan et al.*, 1975].

[13] A simple experiment was conducted using a 17-cm bowtie antenna in free space and on a dielectric half-space consisting of dry sand. The reflection coefficient of the antenna was measured using a network analyzer in both cases to estimate the resonant frequency. The results are shown in Figure 3 with free space indicated by the solid line, and sand indicated by the dashed line. The permittivity of the sand was measured using a dielectric probe to be approximately 2.5. The measurements show a frequency shift from 1.2 GHz to 0.93 GHz, indicating a 22.5% reduction in the resonant frequency. Assuming an effective relative permittivity of 1.75 (mean permittivity between the air and ground) for the half-space, the

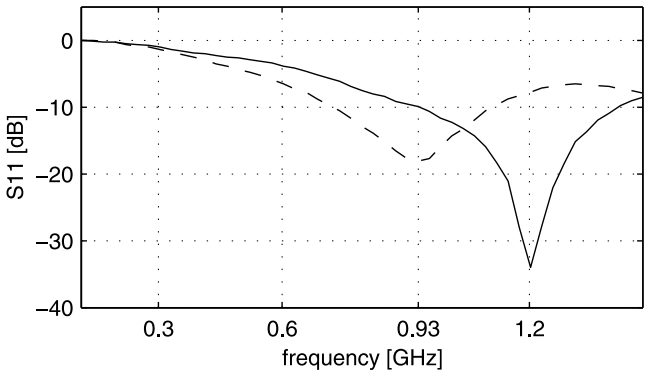

Figure 3. Reflection coefficient [S11] of a 17-cm bowtie (solid) in free space and (dashed) over dry sand.

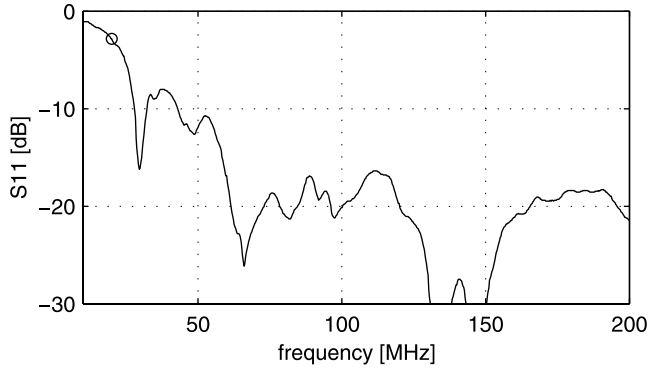

Figure 4. Reflection coefficient [S11] of the 2.6-m bowtie over dry sand. The circle indicates the lower 3-dB cut-off frequency.

predicted reduction is about 24.4%, agreeing with the measurements. In general, the frequency reduction for an antenna placed directly on the surface of the ground will be approximately $1/\sqrt{\varepsilon_{eff}}$, where ε_{eff} is the average permittivity of the ground and air.

2.2.2. Bowtie Antenna (Transmit Antenna)

[14] The bowtie transmit antenna was constructed to operate over the frequency range 10 MHz to 120 MHz. Antennas of the large size required to radiate at the lower frequencies must be collapsible for storage and transportation. An aluminum screen was used since it was lightweight, the fine mesh behaved as a solid conductor over the frequency range of interest, and it could be easily stored for transportation and deployed in the field. In free space, an antenna designed for a center frequency of 10 MHz would need to be 15 m in length. Assuming a 50% reduction in length due to the dielectric loading of the ground, and a usable frequency range of at least 50% below the resonant frequency due to ground loading, the required antenna size becomes 3.75 m. A final design was selected using two 1.3 m equilateral triangles supported by a PVC frame. Preliminary testing of the antennas over dry sand (ε_r = 2.5) with a network analyzer and 4:1-balun transformer showed a 3-dB lower cutoff at about 20 MHz with a resistive impedance around 50 Ω at the input of the transformer (200 Ω input resistance for the antenna [*Compton et al.*, 1987]). Figure 4 shows the reflection coefficient of the antenna versus frequency with the circle at the 3 dB cutoff.

2.2.3. High-Impedance Operational Amplifier/Dipole (Receive Antenna)

[15] The transmit and receive antennas of a ground-penetrating radar system are usually identical. Through reciprocity, if an antenna is a good radiator, it is also a good receiver, and the same antenna used to transmit power into the ground can also be used to collect the reflected power. Also, since the antennas are the bandwidth-limiting components of the system, the highest power transfer is achieved when they are "matched." However, there is a slight difference in the specific roles of transmit and receive antennas concerning power transfer. The transmit antenna must radiate power efficiently into the ground, whereas the receive antenna only needs to measure the incident electric field. Due to this difference, matching the receive antenna for maximum power transfer is not a concern as long as the electric field is being measured. This characteristic is exploited to design a relatively small receive antenna that operates over a large frequency bandwidth.

[16] The effective length is a parameter that is used to describe the radiating and receiving properties of an antenna [*Stutzman and Thiele*, 1981]. For the radiating case, this quantity is equal to the total current-length product on the antenna relative to the current at the antenna feed. For the receiving case, this quantity is equal to the voltage induced upon the terminals when the antenna is open circuited. The effective length of an electrically small dipole is approximately equal to half of the physical length. More importantly, an electrically small dipole can be used for receive if the voltage induced upon the antenna terminals can be measured while the antenna is open circuited. This is accomplished using a high input-impedance, high-bandwidth, operational amplifier in the configuration shown in Figure 5.

2.2.4. Antennas on Mars

[17] The antenna design for a rover on Mars might be the most technically challenging aspect of system development.

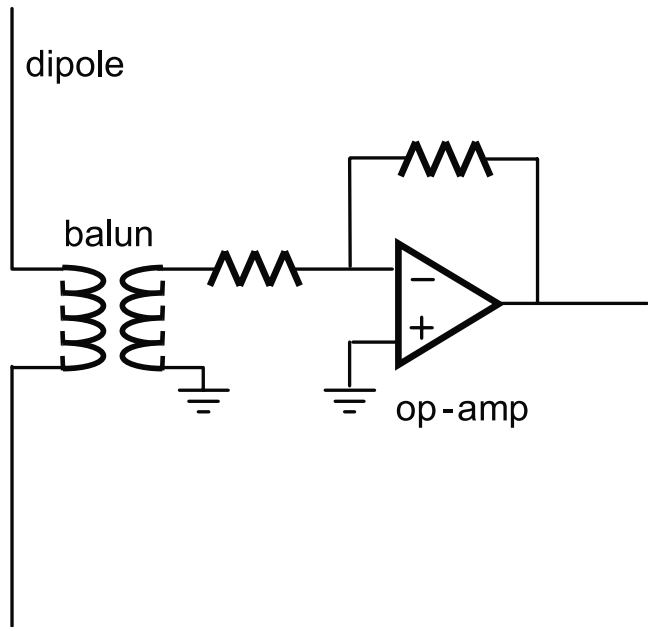

Figure 5. Dipole and high-impedance operational amplifier antenna subsystem.

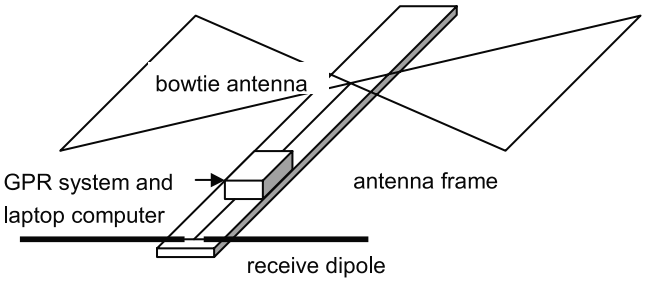

Figure 6. Complete radar system.

The antenna systems described above include a large bowtie transmit antenna and a compact receive dipole. The size of the bowtie will certainly restrict it from operation on a mobile rover; however, the bowtie could be placed on a stationary powered lander and a compact dipole on a mobile rover. The 2009 Mars Smart Lander Science Definition Report [*Arvidson et al.*, 2001] outlines two possible scenarios that would be appropriate for this configuration - one with a powered lander and the other with a geophysics drop package. Either one of these scenarios would provide a means to employ a low-frequency antenna in conjunction with the compact receiver. If the stationary transmit antenna is not a possibility, the frequency of operation for the entire system will need to be increased so the antennas can be mounted on the rover without restricting its movements. It is extremely important that the antennas do not compromise other science experiments.

2.3. Complete System

[18] Figure 6 shows the complete ground-penetrating radar. All the systems, including the transmitter, receiver, antennas, batteries, and laptop, are mounted on a wooden ski/sled that can be dragged as data are being collected. The bowtie antenna is located at the rear of the ski and is supported by a PVC frame. The transmitter is placed very close to the bowtie antenna to reduce any multiple reflections caused by the mismatch of the transmit antenna. The receive antenna is placed as far as possible on the ski from the bowtie to reduce the antenna feed-through signal. The choice of ski length is important when considering the amount of feed-through that can be tolerated. A large ski would provide greater separation at the cost of a less mobile system. For initial testing, a 2.7-m board was used. The transmitter/receiver box, laptop computer, and batteries are located between the antennas on the ski. The entire system is portable and requires no external power or control cables.

3. Experiments

[19] To evaluate the performance of the prototype system, field experiments were collected at one site in Lawrence, Kansas, and others near Fairbanks, Alaska. For most of these experiments, data were collected over stratigraphy that was, to some extent, already determined through seismic surveys, dilled cores, or other geological surveys. This information was extremely valuable in interpreting the data and, in a few cases, was used to simulate radar responses for data interpretation. This section begins with a description of the preliminary field experiment in Lawrence, Kansas. This field experiment was intended to provide a basic check on the operation of the system. Next, the results from field experiments in Alaska are presented. For two of these experiments, simulated results are gen-

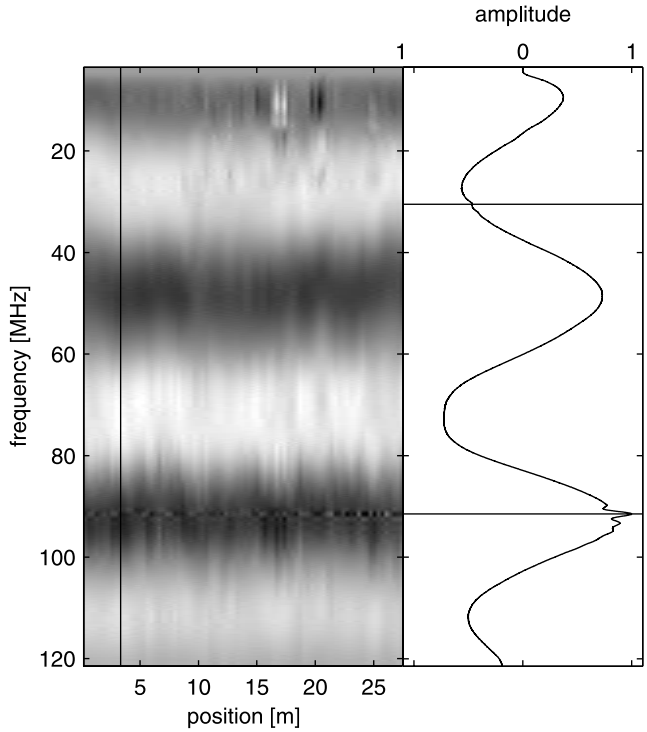

Figure 7. Raw data collected in the west campus of the University of Kansas.

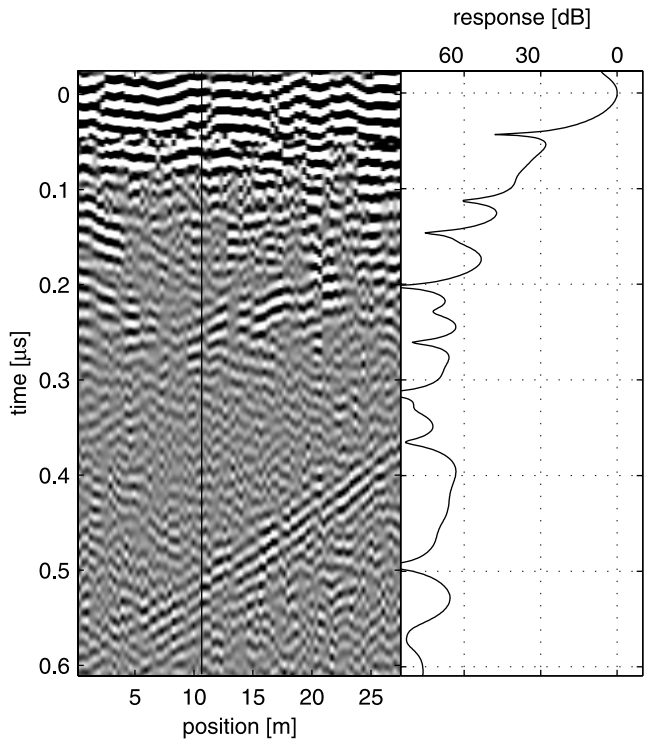

Figure 8. Processed image and normalized amplitude plot [dB] of the data collected in Lawrence, Kansas.

Table 2. Stratigraphy of the Test Site in Delta Junction

Depth	Lithology	ϕ%	s%	Fill
0.2	air	100	–	–
0.6	silt (eolian deposit)	30	70	water
1.4	silt (eolian deposit)	20	100	ice
–	gravel (out wash)	30	0	–

erated and compared with the experimental results to help interpret the data.

3.1. Lawrence, Kansas

[20] The first experiment was conducted outside Moore Hall (Kansas Geological Survey) on the west campus of the University of Kansas. The main objective was to test the basic operation of the system and identify any problems that might be encountered during future experiments in Alaska. The site was selected because, previous to the radar measurements, a seismic survey had been conducted by the Kansas Geological Survey [*Knapp*, 1990]. This information are compared with the radar measurements to provide some geological context. The main target of interest is a layer of limestone at about 5 m depth. This layer provided a target that was sufficiently deep to be resolved from the surface response, and shallow enough to provide a strong backscattered signal.

[21] Radar measurements were collected over a traverse of approximately 30 m with a sample interval of about 0.33 m between traces. The radar system had not yet been automated for this experiment, requiring the user to manually trigger the system and save the data to disk at each trace location. The raw data are displayed in Figure 7. For clarification, the vertical axis of this figure indicates the instantaneous transmit frequency as the radar sweeps from 5 MHz to 120 MHz. The dominating sinusoidal response is the beat frequency associated with the antenna feed-through. Two important features can be noticed in the unprocessed data. First, there exists significant transmitted and received power over the entire frequency range of 5 MHz to 120 MHz. This indicates that both the bowtie and operation amplifier-dipole antenna subsystems are efficiently transmitting power and measuring the reflected field over more than four octaves of the frequency spectrum. Second, two external noise sources are detected at 91.5 MHz and 30.5 MHz, as shown by the horizontal lines in the amplitude plot on the right of the figure. The noise is attributed to a local FM radio station, KANU, at 91.5 MHz. The component at 30.5 MHz is a nonlinear effect of the receive mixer, and similar interference components will be seen at the other odd harmonics of 91.5 MHz, including 18.3 MHz, 13 MHz, and so on.

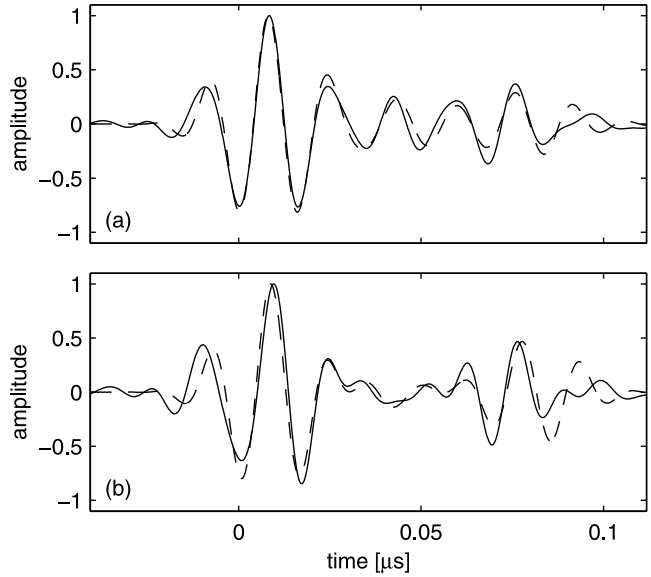

Figure 10. FDTD simulated waveform comparison of the data at the (a) 6-m position and (b) 20-m position.

[22] A radar profile is generated from the raw data through a number of signal processing steps. The time response is obtained by evaluating the beat frequency spectrum of the collected data via an inverse Fourier transform. Prior to transforming the data, the limits of the transform must be determined, and a windowing function is applied to reduce sidelobe levels. Due to the radio interference, the limits of the transform were selected to range from 30.5 MHz to 91.5 MHz. Next, a Hanning window [*Harris*, 1978] is applied and an IFFT is performed. A "dewow" filter [*Sensors and Software, Inc.*, 1996] is used to remove any DC bias and bring out the higher frequency events. To help increase the signal-to-noise ratio, a number of traces can be added coherently, but due to the relatively large separation between traces in this experiment, only a few integrations could be tolerated before some of

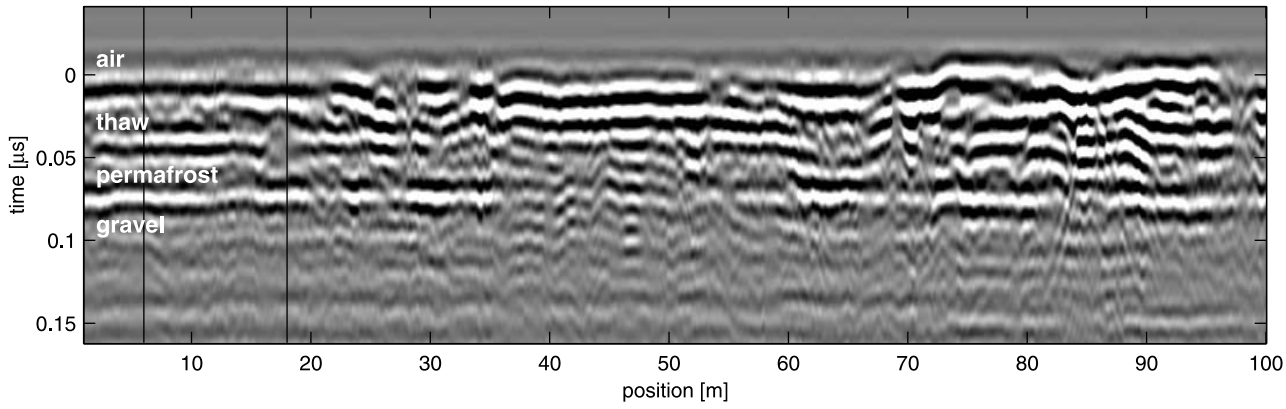

Figure 9. Processed image of the data collected in Delta Junction, Alaska.

Table 3. Estimated Depth and Electrical Properties at the 6 m Position

Depth	Lithology	ε_r	σ, S/m
0.2	air	1	–
1.2	silt (eolian deposit)	18	0.02
2	silt (eolian deposit)	9	0.001
–	gravel (out-wash)	3	–

the more steeply dipping events were deteriorated. Finally, a gain function is applied to the data to amplify the deeper reflection that experienced more attenuation due to spherical spreading and other losses. The processing steps are listed below and the final image is shown in Figure 8.

[23] Basic Signal Processing Steps

1. Choose FFT limits.
2. Apply windowing function.
3. Transform data.
4. Differentiate/dewow/high pass filter.
5. Average/stack/integrate.
6. Apply gain.

[24] A few events can be noticed in the processed GPR image. The antenna coupling and surface response occur at 0 μs, and show significant ringing for about 0.7 μs. At approximately 0.08 μs, a reflection occurs across the entire image just below the antenna feed-through and surface response. This event is distinguished from the surface response since it does not follow the same pattern along the traverse. A similar event is shown just below at approximately 0.15 μs. These two reflections seem to indicate the upper and lower boundarys an Amazonia limestone member [*Knapp*, 1990]. The amplitude plot on the right is used to estimate the resolution and dynamic range of the system. The temporal resolution is estimated to be on the order of 0.03 μs, and the dynamic range is at least 70 dB. Two more events appear around 0.2 to 0.3 μs. The longer one follows a hyperbolic curve indicating a somewhat localized scatter at the 22 m position and 0.2 μs time delay. It is difficult to explain this reflection in more detail without addition resources such as a drilled core. The final highlighted reflection occurs from 0.6 μs to 0.4 μs moving from left to right. The slope of this reflections is consistent with the air wave from an object on the surface such as a building. This type of surface clutter is a result of using non-shield antennas, normally not the case with commercial GPR systems. For a rover on Mars, the antennas will not be sheilded due to mass requirements, and surface clutter from rocks might be a problem depending on their size and distribution.

3.2. Alaska

[25] From August 19th to August 31st of 2001, field experiments were conducted in Alaska. The major goals were to verify the performance of the system and to evaluate the use of ground-penetrating radar to detect permafrost and the presence of water or ice within permafrost. The ambiguities associated with using a radar to detect subsurface deposits of ice or water can be investigated through these surveys. Unfortunately, due to the time of year, a significant amount of rain fell before and during the experiments. Due to this large amount of precipitation, the upper meter or so of the test sites (known as the "active layer") was saturated with water. This upper saturated layer most likely decreased the backscattered power from deeper objects by a considerable amount due to the increased attenuation.

Table 4. Estimated Depth and Electrical Properties at the 20 m Position

Depth	Lithology	ε_r	σ, S/m
0.2	air	1	–
0.5	silt (eolian deposit)	18	0.02
2.4	silt (eolian deposit)	9	0.001
–	gravel (out wash)	3	–

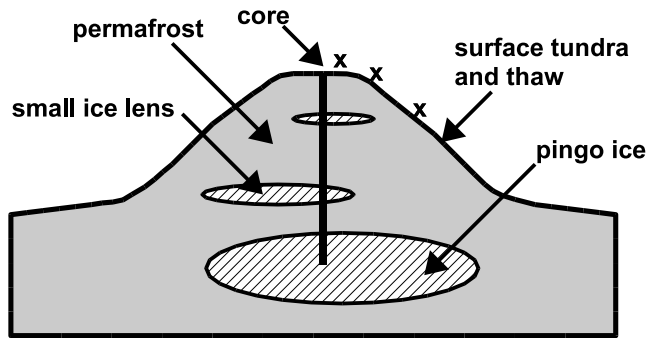

Figure 11. Interpretation of the pingo subsurface structure with radar sample locations indicated by the x's.

3.2.1. Delta Junction

[26] On August 21st, measurements were collected at a site in Delta Junction, a city about 100 miles west of Fairbanks. The stratigraphy of the test site, as shown by Table 2, includes layer of silt (eolian deposit) above an outwash layer of gravel. The layer of silt is broken down into a near-surface thaw layer and a layer of permafrost extending down to the gravel. Due to the high water saturation of the upper thaw layer, a relative permittivity of 20 with relatively high loss is assumed. The frozen silt has a considerably smaller dielectric of around 6 and less attenuation.

[27] At the test site, 1000 traces were collected at a spatial frequency of around 10 traces per meter for a total length of 100 m. A significant band of interference is noticed up to 35 MHz, most likely resulting from CB radios. As a result, the limits of the Fourier transform were selected to extend from 35 MHz to 120 MHz. The processed image is shown in Figure 9. The reflections indicate a somewhat continuous layer occurring across the entire image at 0.075 μs. Using Table 2 as a reference, it is probable that this reflection is a

Table 5. Pingo Stratigraphy and Lithology

Depth	Lithology	ϕ%	s%	Fill
0.2	air	100	0	–
0.3	tundra	50	70	water
0.5	soil, eolian deposit	40	70	water
1.0	soil	30	90	ice
0.5	ice	100	100	ice
4.0	soil	30	90	ice
0.5	ice	100	100	ice
0.5	soil	25	90	ice
?	ice (main pingo ice)	100	100	ice

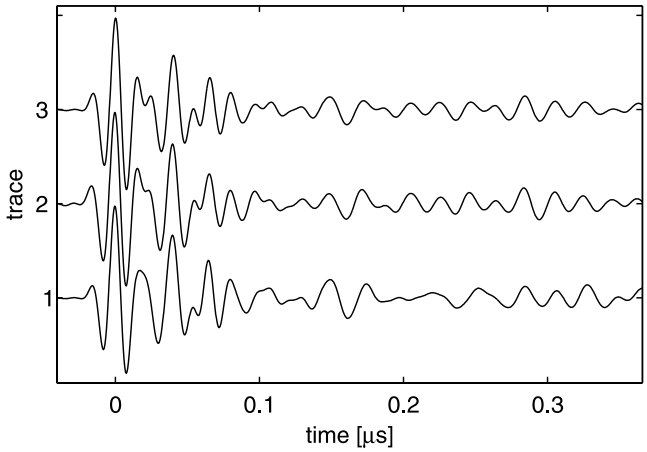

Figure 12. Radar responses at the three locations at the pingo site.

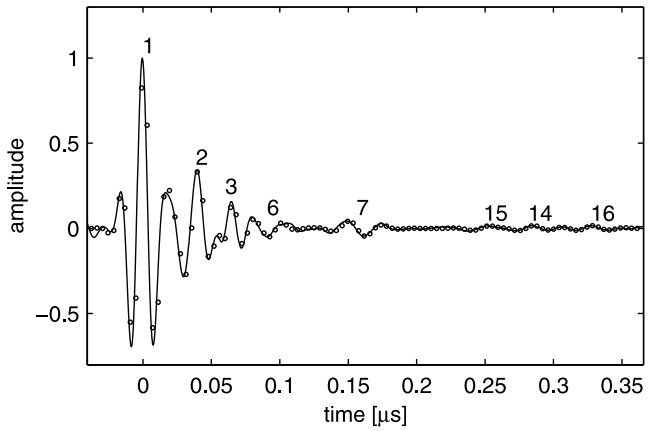

Figure 13. Waveform comparison using the reflection profile in Table 6.

result of the silt-gravel interface occurring at 3 m. There is a less continuous reflection above this reflection that ranges from 0.03 μs to 0.05 μs. Again referring to Table 2, this reflection is possibly a result of the transition between the active thaw layer and the more permanent frozen layer of the near-surface eolian silt deposit. The depth fluctuations are likely due to varying degrees of sunlight incident on different areas along the traverse. Another features in the image include a discontinuity of the silt-gravel interface from 40 m to 60 m.

3.2.1.1. Data Interpretations

[28] Radar simulations were used to help identify the subsurface layering and reinforce the interpretations mentioned above. The simulation model is similar to the stratigraphy described in Table 2. The finite difference time domain [*Yee*, 1966] (FDTD) method was preferred as the simulator for a number of reasons. First, due to the proximity of the radar system to the surface and subsurface layering, spherical propagation must be considered, and therefore, a two- or three-dimensional simulator should be used. Second, the FDTD method is able to account for the half-moon-shaped radiation pattern of an antenna placed over a layered-dielectric half-space [*Annan et al.*, 1975]. The amount of computation time required to simulate the radar response of the chirp signal using FDTD would have been extremely large, and, therefore, it was more reasonable to simulate the response of an implusive system. The response of a frequency-modulated system was still be obtained by performing the pulse compression prior to the simulation rather that after. By generating the pulse in this manner, the sidelobes associated with a frequency domain system will be included in the simulation.

[29] The FDTD mesh contains all the spatial information for the simulation, such as the physical dimensions, boundary locations, and electrical values. For the simulations, the mesh is a 200-by-200-cell, two-dimensional grid with a cell size of 8 cm by 8 cm. The ground extends from cells 101 to 200 and is divided into three layers with initial permittivities of 20, 8 and 5, corresponding to the thawed eolian deposit, frozen eolian deposit and gravel out-flow layers, respectively. The initial conductivities for the eolian deposits are 0.015 S/m for the thaw layer and 0.002 S/m for the frozen layer. The transmitter and receiver are positioned at grid locations (99,105) and (99,130) respectively.

[30] Two responses were generated for the case of a three-layer model containing an active-thaw silt layer, a frozen silt layer, and an out-flow gravel layer. For both simulations the silt-gravel interface was at a depth of around 3 m, and locations for the thaw-frozen silt interface were varied to match the data. The simulations are intended to represent two possible cases that correspond to the data at the 6-m and 18-m positions as indicated by the vertical lines on Figure 9. The depth of the intermediate freeze-thaw interface is easily detected at the 6m position; however, this layer seems to disappear around 18 m. For each simulation, the values of the electrical properties and depth to the interface are iterated to obtain a match with the actual data. The results of the first simulation are shown in Figure 10a along with the actual data. The resulting permittivities and loss factors are shown in Table 3. There is a very close match reinforcing the likelihood of the freeze-thaw interface. The disagreement at greater time delays is most likely caused by an incorrect assumption that only three layers with discrete permittivity changes are present. The results and values for the second simulation are shown in Figure 10b and Table 4.

[31] The simulation results seem to indicate that the freeze-thaw interface is closer to the surface at the 18-m position than at the 6-m position. This information could not be directly derived from the image alone, since this layer could not be adequately resolved from the antenna coupling and surface response. Instead, by replicating the near-surface interference pattern using FDTD, the layering could be identified. Furthermore, this layer is most likely continuous

Table 6. Results of the GPR Response

Iteration	Time, μs	Amplitude	f_c, MHz	BW, MHz
1	0.04	1.000	58	33
2	0.08	0.345	49	24
3	0.101	0.174	67	33
6	0.132	0.050	47	28
7	0.197	0.049	39	23
14	0.322	0.016	43	24
15	0.290	0.016	35	28
16	0.368	0.016	41	23

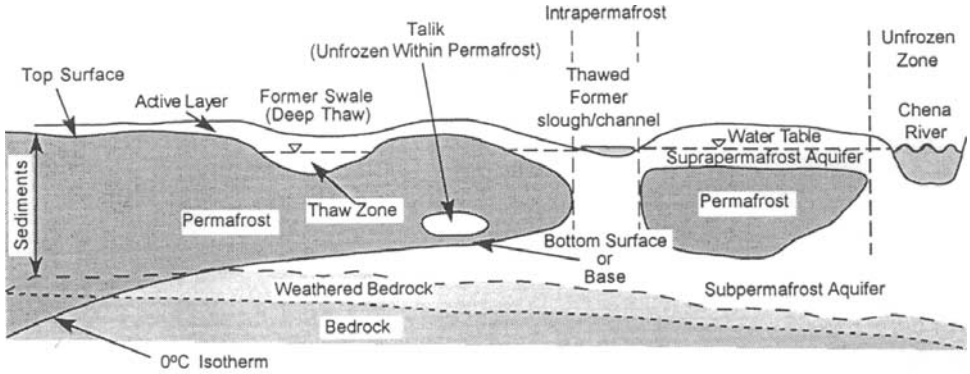

Figure 14. Interpretation of the subsurface structure at Fort Wainwright.

across the entire traverse, but due to varying degrees of depth and permittivity contrast it is not as noticeable as the silt-gravel interface.

3.2.2. Pingo Site

[32] An experiment was conducted at a pingo site to investigate the use of radar to detect subsurface deposits of ice. Pingos have been identified as a possible indication of water on Mars [*Squyres et al.*, 1992]. A pingo is a subsurface ice lens that has formed through an upward flow of water from an underground source. Before the water can reach the surface, it freezes forming a lens of relatively pure ice. This upward flow of water and subsequent freezing elevates the surface and produces a small hill. Due to this elevation, it is fairly easy to locate a pingo by looking for a group of trees that appear to be higher than their surroundings.

[33] The area on and surrounding the pingo site was dense with underbrush and trees. Due to the large amount of trees and plants, access to the location was difficult and collecting data over a traverse was practically impossible. As a result, data collection was restricted to a few discrete locations often separated by a meter or more. A core had been drilled at the peak of the site to provide additional information concerning the structure of the subsurface. This information is valuable in interpreting the responses collected by the radar system. Using data from the core measurements, the stratigraphy and lithology of the first pingo are shown by Figure 11 and listed in Table 5.

3.2.2.1. Data Interpretation

[34] The three radar responses corresponding to the x's in Figure 11 are shown in Figure 12. A linear gain is applied to bring out some of the deeper events. Several reflections are present within these waveforms, and there seems to be a general trend of a decrease in center frequency and bandwidth from the deeper reflections. This is not unusual, as one would expect increased attenuation at higher frequencies. With the Delta Junction sites, FDTD simulations were used to find a match for the measurements and aid in data analysis. For the pingo site, iterating over the 9 or more layers with FDTD is impractical and time consuming. As an alternative, a reflection profile are obtained directly from the data and a simulated waveform is generated using an iterative process [*Leuschen*, 2001]. From the reflection profile, possible locations of the ice lens can be identified.

[35] The iterative routine was applied to the first trace, and a comparison with the simulated response is shown in Figure 13 with no gain applied. The corresponding reflection profile is listed in Table 6. The first column of Table 6 is the iteration number, some of which are not listed. The table only contains the internal reflections that are selected by evaluating the time, amplitude, and frequency content of each reflection. In general, a reflection from a deeper interface will show increased attenuation and lower frequency content. The far-right column of Table 6 illustrates this behavior, as the center frequency of the reflected pulse decreases with increasing time delay. Reflections that appear to contain reasonable amplitude, time delay, and center frequency are selected as subsurface reflections. The other waveforms are most likely errors from the decomposition process, multiple reflections, system artifacts, or reflections from trees and other sources of clutter.

[36] Two of the reflections listed in the tables seem to indicate the top and bottom of the pingo. The first is around 0.15 to 0.16 μs and has an amplitude of about 0.05 compared to the surface response. The second is around 0.28 to 0.29 μs and has an amplitude of about 0.04. With an average dielectric of 8, these reflections would relate to a range of around 8 m and 15 m, respectively, along the same scale as recorded from the core measurements for the top of the pingo. The fact that the amplitude of the second reflection is close to that of the first would indicate a relatively low-loss dielectric for the layer between the reflections. This also agrees well with the dielectric properties of pure ice at the radar frequencies.

3.2.3. Fort Wainwright

[37] The final experiment in Alaska was conducted at Fort Wainwright near Fairbanks. We accessed the site using

Figure 15. GSSI radar system including antennas and tracked vehicle. The prototype system is shown in the upper left.

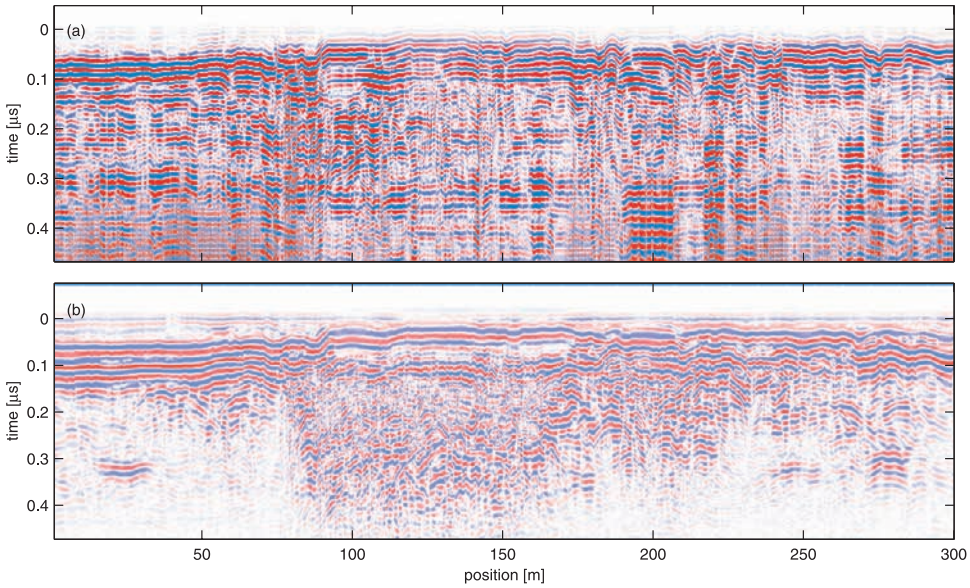

Figure 16. Processed images of the data collected along the 300-m line for the (a) prototype system and (b) GSSI system.

a tracked vehicle that was able to navigate across mud and cross small ponds. The site contained a 4-ft-wide line cut through a spruce forest and was approximately 300 m in length before it intersected a small pond resulting from recent flooding. From previous radar surveys and drilling, the subsurface of this location is thought to consist of a near-surface saturated thaw layer overlying discontinuous permafrost, as shown in Figure 14. Beneath the permafrost could lie a small layer of wet soil above the water table and bedrock.

[38] The radar results were compared with those collected with an "impulse"-type commercial Geophysical Survey Systems, Inc. (GSSI) System 10B control unit and CD10A video display [*Arcone et al.*, 2001]. The antenna subsystems for this unit were two 50-MHz resistively loaded dipoles attached to a standard GSSI 100-MHz transmitter and receiver as shown in Figure 15. An image of the prototype system is also included in this figure as a comparison. To reduce cable noise, the transmitter and receiver were connected with a fiber optical link. With a combined weight of well over 100 kg, the antennas were dragged 5 m behind the tracked vehicle. Also, a larger antenna separation of 4.6 m (more than twice the distance used with the FM-CW system) was used to avoid saturating the receiver.

[39] Data were collected continuously along the 300-m traverse with the prototype system. The spacing was approximately 3 cm per trace for a total of 10000 traces. Once again, external noise sources limited the lower frequency band to about 30 MHz prior to the Fourier transform. A few additional signal-processing steps were applied to the data after converting to the time domain. First, any DC bias was removed, and the traces were equalized by normalizing by the standard deviation. Next, the mean value across the traverse at each time step was removed to reduce any coherent system effects within the data. Finally, the data were coherently integrated by convolving them with a 16-value Hanning window. The processed image is shown in Figure 16a.

[40] Several events can be detected in the image. The first is the continuous reflection ranging from about 0.3 μs to 0.35 ns. This reflection ranges from 0 m to 50 m at 0.3 μs, slowly decreases from 50 m to 70 m, and then extends from 70 m to 150 m at about 0.35 μs. This layer is picked up again at around 190 m and is seen off and on to the end of the traverse. It is possible that this reflection indicates the transition from the permafrost to a wet soil. Beneath this reflection at about 0.41 μs is a relatively flat layer extending from 0 m to 80 m. There is also a weaker reflection around 0.4 μs from 100 m to 150 m. Due to the flat characteristics of these layers, they could indicate a water table existing below the permafrost. This layer may disappear as the permafrost becomes deeper and extends into the water table. There seems to be many near-surface events within the image. The most prominent shown across the entire image is the ringing of the near-surface active thaw layer.

[41] The processed image for the commercial system is shown in Figure 16b. The data were collected along the same line as the previous image. Some of the same features seen in Figure 16a can also be noticed in this image. First, the response just below the antenna coupling is evident in both images and shows a similar trend. In Figure 16a, this response is level from 0 to 50 m and then begins to rise until about 120 m. Figure 16b shows the same response. The interface between the permafrost and saturated soil occurring at approximately 0.35 μs can also be noticed in both images.

3.2.3.1. Bistatic Measurements

[42] Bistatic measurements were also collected as an example to show how the antenna configuration could be used with stationary lander and mobile rover. The data were collected by keeping the large bowtie stationary and moving the compact dipole from a distance of 4.8 meters away toward the bowtie. The processed data are shown in Figure 17. Two events are indicated by dashed lines in the figure. The top line indicates the air wave and the bottom

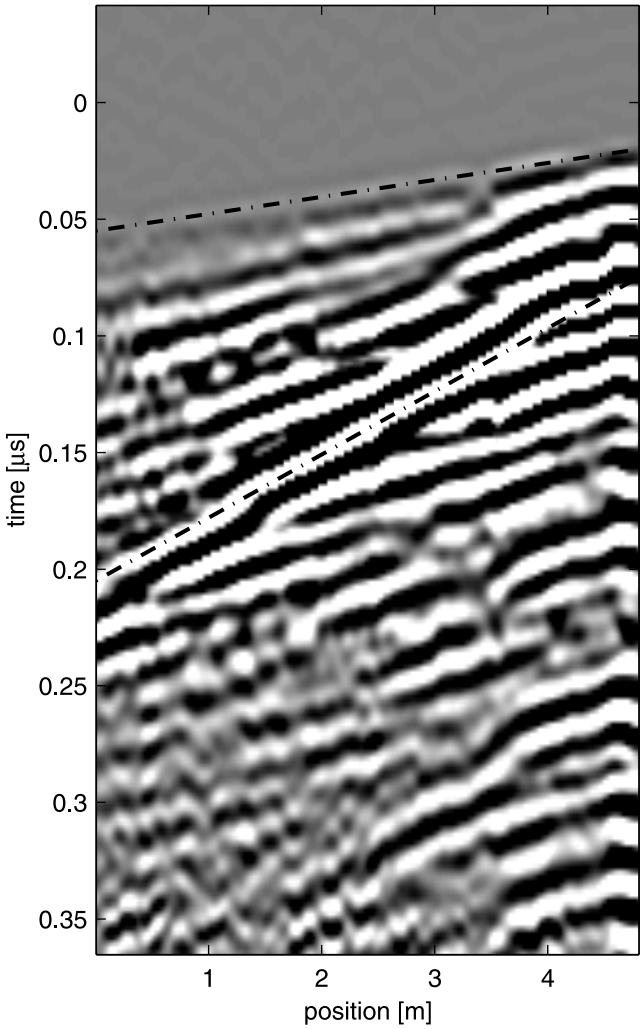

Figure 17. Bistatic measurements collected with the prototype system.

line indicates the reflection off of the thaw/permafrost interface. With velocity analysis, the permittivity and depth of the thaw layer can be calculated to be approximately 16.1 and 1.7 m, respectively. These numbers agree well with what would be expected at this site and also with the data interpretations from the Delta Junction experiments.

4. Conclusions and Future Work

[43] This paper presents a lightweight, low-power, rover/lander-based system intended to probe the subsurface of Mars to a depth of 100 m. In relatively poor conditions, the system was able to detect dielectric interfaces up to 30 m, and showed similar results when compared to a commercial system that was not designed with power and weight restrictions. Furthermore, the likelihood of experiencing the same levels of water saturation in the upper layers of Mars as experienced in the presented field work is nearly impossible, and a similar system should be able to penetrate much deeper. However, this does not take into account any magnetic losses that could significantly reduce penetration depth. We believe that under favorable conditions a similar GPR on Mars could detect structures as deep as a hundred meters, but as the ohmic and scattering losses increase penetration depth will be greatly reduced.

[44] Based on these results, we propose an FM-CW system operating from a few megahertz to a few hundreds of megahertz for a lander/rover-based mission. With some modifications to the existing transmitter, a radar system operating from 5 MHz to approximately 500 MHz could be easily developed. This type of system would be the most likely to acquire useful information, as it would be able to achieve both high resolution near the surface and deep penetration. Of course, the final system design will depend on the rover characteristics and the size of antenna that can be accommodated on the rover or lander.

[45] This research has shown that a lightweight, low-power system can be easily built to meet the size and weight requirements of a Mars mission, and can operate over a wide enough frequency band to ensure reasonable penetration depth without sacrificing resolution. Using a high-speed digital synthesizer and a simple receiver design, the entire system could be incorporated into a single multilayer PCB with surface-mount components. Also, the antenna subsystems presented in this paper include a relatively small, mobile dipole receive antenna that could be used in conjunction with a mobile/stationary bowtie to perform either monostatic or bistatic measurements. Future improvements to the system include increasing the bistatic capabilities of the system by replacing the receive antenna cable with a more mobile RF link. If this was done, the receiver (ideally placed on a rover in this case) would have the ability to move freely without needing to support the large transmit antenna or a cable link. Additionally, the majority of the power consumption required by the transmitter would be available from the lander, not the rover.

References

Annan, A. P., W. M. Waller, D. W. Strangway, J. R. Rossiter, J. D. Redman, and R. D. Watts, The electromagnetic response of a low-loss, 2-layer, dielectric earth for horizontal electric dipole excitation, *Geophysics*, *40*(8), 285–298, 1975.

Arcone, S., C. Leuschen, and S. P. Gogineni, Comparative permafrost radar tests: Fairbanks, Alaska, CRREL report, Cold Reg. Res. and Eng. Lab., Hanover, N. H., 2001.

Arvidson, R. E., et al., NASA Mars Exploration Program Mars 2007 Smart Lander Mission Science Definition Team Report, NASA Headquarters, Washington D. C., 2001.

Compton, R. C., R. C. McPhedran, Z. Popovic, G. M. Gebeiz, P. P. Tong, and D. B. Rutledge, Bow-tie antennas on a dielectric half-space: Theory and experiment, *IEEE Trans. Antennas Propag.*, *35*(6), 622–631, 1987.

Davis, J. L., and A. P. Annan, Ground-penetrating radar for high-resolution mapping of soil and rock stratigraphy, *Geophys. Prospect.*, *37*, 531–551, 1989.

Fujimoto, K., A. Henderson, K. Hirasawa, and J. R. James, *Small Antennas*, John Wiley, New York, 1987.

Harris, F. J., On the use of windows for harmonic analysis with the discrete Fourier Transform, *Proc IEEE*, *66*(1), 51–83, 1978.

Knapp, R. W., Vertical resolution of thick beds, thin beds, and thin bed cyclotherms, *Geophysics*, *55*(9), 1183–1190, 1990.

Leuschen, C., Surface-penetrating radar for Mars exploration, dissertation, Univ. of Kan., Lawrence, 2001.

Sensors and Software, Inc., *Pulse Ekko Tools User Guide Version 1.22*, *Tech. Manual 22*, Mississauga, Ontario, Canada, 1996.

Squyres, S. W., S. M. Clifford, R. O. Kuzmin, J. R. Zimbelman, and F. M. Costard, Ice in the Martian regolith, in *Mars*, edited by H. H. Kieffer et al., pp. 557–593, Univ. of Ariz. Press, Tucson, 1992.

Stutzman, W. L., and G. A. Thiele, *Antenna Theory and Design*, John Wiley, New York, 1981.

Yee, K. S., Numerical solution of initial boundary-value problems involving Maxwell's equations in isotropic media, *IEEE Trans. Antennas Propag.*, *14*, 302–307, 1966.

S. Arcone, USACE Engineer Research and Development Center, Cold Regions Research and Engineering Laboratory, 72 Lyme Road, Hanover, NH 03755, USA.

P. Gogineni and P. Kanagaratnam, Radar Systems and Remote Sensing Laboratory, University of Kansas, 2335 Irving Hill Road, Lawrence, KS 66045, USA.

C. Leuschen, Applied Physics Laboratory, Johns Hopkins University, 11100 Johns Hopkins Road, Laurel, MD 20723, USA. (Carl.Leuschen@jhuapl.edu)

K. Yoshikawa, Water and Environmental Research Center, Institute of Northern Engineering, University of Alaska, Fairbanks, P.O. Box 755860, Fairbanks, AK 99775, USA.